HaloSat Observation of the Virgo Intracluster Medium*

Nathan H. Hewitt [1], Philip Kaaret [1,†] and Chase A. Fuller [1]

[1] Department of Physics and Astronomy, University of Iowa, Iowa City, IA 52242

ABSTRACT

Contained within a galaxy cluster, the Intracluster Medium is comprised of hot, X-ray emitting material between member galaxies. The nearest (∼16.1 Mpc) large galaxy cluster is Virgo. Virgo covers an approximately 12° diameter field, making it challenging to observe in its entirety. The HaloSat satellite utilized a 7° radius field of view to obtain the first full cluster observations since 1994. We then fit the cluster spectra with a plasma emission model of fixed metallicity. Our best fit temperature is $kT = 1.39 \pm 0.11$ keV. We report a cluster luminosity of $5.8 \pm 0.7 \times 10^{43}$ erg s^{-1} and an emission measure of $5.8 \pm 0.6 \times 10^{66}$ cm^{-3}.

Keywords: X-Ray Astronomy (1810) — X-Ray Sources (1822) — Virgo Cluster (1772) — Intracluster Medium(858) — Galaxy Clusters(584)

1. INTRODUCTION

The Virgo Cluster is the closest large galaxy cluster, found within the namesake Virgo constellation. The cluster is composed of over 1000 member galaxies, located about 16.1 Mpc from Earth (Tonry et al. 2001) with an approximately 6° radius (de Vaucouleurs 1961). Virgo's Intracluster Medium (ICM) is contained within the cluster's gravity while considered external to individual member galaxies. Virgo's ICM produces distinct X-ray emissions of an X-ray surface brightness profile with an unusually shallow radial dependence, implying a large contribution from outer material. Comprehensive X-ray observations of the cluster are challenging due to its large angular size, with recent studies from Urban et al. (2011) and Su et al. (2019) constrained by limited detector view-fields. The HaloSat mission represents the first full survey of this intergalactic feature since ROSAT in Böhringer et al. (1994), which provided poor energy resolution. The following analysis seeks to measure the temperature and total X-ray luminosity of Virgo's ICM by analyzing a single X-ray spectrum of the entire cluster.

2. OBSERVATIONS

Three collimated silicon drift detectors (SSD) comprise HaloSat. Each SDD possesses a field of view reaching a 5° radius, tapering to zero response past 7° (Kaaret et al. 2019). The instrument is sensitive to X-rays from 0.4-7.0 keV. Background events were filtered by applying thresholds of 0.16 s^{-1} and 0.75 s^{-1} to the hard-band (3.0-7.0 keV) and Very Large Event (>7.0 keV) rates respectively. We observed an average clean exposure of 13.1 ks per detector, with a total of 4798 surviving events.

Data analysis was conducted using version 12.11.1 of the X-Ray Spectral Fitting Package XSPEC (Arnaud 1996). We modeled our X-ray spectra as $\texttt{Apec}_{LHB}$ + $\texttt{Tbabs}(\texttt{Powerlaw}_{CXB}$ + $\texttt{Apec}_{GH}$ + $\texttt{Apec}_{V})$ using abundances from Wilms et al. (2000). The `Apec` model describes the emission spectrum of collisionally-ionized diffuse gas (Smith et al. 2001), the `Tbabs` model described interstellar absorption (Wilms et al. 2000), and `Powerlaw` is a simple, analytic model of form E^{-n} and photon index n. Subscripts are included to distinguish components' physical origins. Virgo's ICM ($\texttt{Apec}_V$) was modeled using a red-shift $z = 0.00436$ from central galaxy M87 and metallicity $Z_0 = 0.234$ from Urban et al. (2011), as discussed in Sect. 3.

All distant X-ray emissions traverse the Interstellar Medium (ISM) and are dulled by its absorption. Component `Tbabs` sums the cross-section of X-ray absorption over all phases of the ISM (Wilms et al. 2000), and is applied to all non-local model components. We calculated an effective neutral hydrogen column density $n_H = 2.62 \times 10^{20}$ cm^{-2} using the dust map by Planck Collaboration et al. (2014) and the Zhu et al. (2017) conversion factor.

* Citation: Nathan H. Hewitt et al 2021 Res. Notes AAS 5 185

† Corresponding author, philip-kaaret@uiowa.edu

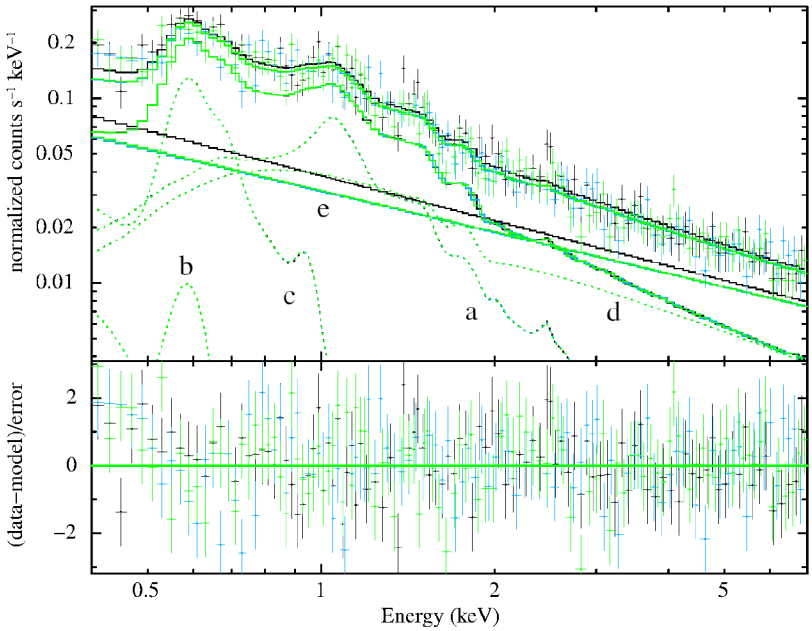

Figure 1. HaloSat spectra of the Virgo Cluster. Data are shown from all three detectors. The solid curves passing through the data points are the summed contributions of every model component, including both the astrophysical and instrumental models. The curve just below the data points is the sum of the astrophysical emission. The spectral components are (a): The Virgo ICM, (b): Local Hot Bubble, (c): Galactic Halo, (d): Cosmic X-ray Background, (e): Particle Induced Detector Background, (Lower solid curve): Astrophysical Model, (Upper solid curve): Full Model Summation.

We introduce component $\texttt{Apec}_{GH}$ to model the Galactic Halo (GH). The GH temperature is best estimated at $kT = 0.17 \pm 0.07$ keV with a normalization $= 0.81 \pm 0.12$. The diffuse Cosmic X-ray Background (CXB) was modeled using a `Powerlaw`, with a photon index of 1.45 from Cappelluti et al. (2017). The Local Hot Bubble (LHB), an approximately 100 pc region of gas surrounding the solar system, produces local, unabsorbed X-Ray emissions. We introduce component $\texttt{Apec}_{LHB}$ to model this gas, adopting a temperature $kT = 0.097$ keV and emission measure from Liu et al. (2017). Particle-induced detector backgrounds (PIDB) were accounted for using a `Powerlaw` model, with respective photon indexes calculated from the hard band count rate according to https://heasarc.gsfc.nasa.gov/docs/halosat/analysis/back20210209.pdf.

3. DISCUSSION

The model produced a good fit with χ^2/d.o.f = 319.43/314. Virgo's best fit temperature was $kT = 1.39 \pm 0.11$ keV, compared to a weighted average $kT = 1.83$ keV calculated from Urban et al. (2011). Urban's team strung together a linear chain of 13 overlapping XMM-Newton observations in the 0.5-2.0 keV band, starting from the central galaxy to the cluster's virial radius (∼4.5°). One could, in principle, derive overarching cluster properties by assuming circular symmetry. However, the presence of bright sub-clusters (M49, M86, M88), weakens this assumption. XMM-Newton is additionally plagued by instrumental Al and Si fluorescence, forcing Urban et al. (2011) to omit events between 1.2-1.8 keV, where we find Virgo brightest. Urban reported an inverse correlation between temperature and radius, observing decreasing temperature outwards from the cluster center. This information, coupled with HaloSat's larger 7° view-field, suggest our lower observed temperature is reasonable.

Freeing the Virgo abundance produced a marginal fit improvement of χ^2/d.o.f = 315.61/313 and metallicity of $Z = 0.11^{+0.10}_{-0.05}$. If the ICM possesses clumps, as suggested by Urban et al. (2011), this is likely an underestimate of Virgo's true metallicity as a single temperature fit over multi-temperature plasma is known to underestimate metallicity.

From our best-fit normalization, Virgo's emission measure (EM) was calculated to $EM = 5.8 \pm 0.6 \times 10^{66}$ cm^{-3}. The unabsorbed flux was calculated over a range of 0.001-100 keV to estimate the bolometric flux $F = 1.9 \pm 0.2 \times 10^{-9}$ erg s^{-1} cm $^{-2}$ and cluster luminosity $L = 5.8 \pm 0.7 \times 10^{43}$ erg s^{-1}. Updating Böhringer et al. (1994)'s luminosity

of 8.3×10^{43} erg s^{-1} with improved distance (20 $\rightarrow$ 16.1Mpc) produces a luminosity of 5.4×10^{43} erg s^{-1} over the 0.1-2.4 keV band. Over the same band we report a value of $5.1 \pm 0.7 \times 10^{43}$ erg s^{-1}. HaloSat provides superior energy resolution compared to ROSAT and therefore an improved estimate of total X-ray luminosity of the Virgo cluster.

This work represents partial fulfillment of a superlative summer research curriculum at the University of Iowa for Nathan Hewitt.

REFERENCES

Arnaud, K. A. 1996, in Astronomical Society of the Pacific Conference Series, Vol. 101, Astronomical Data Analysis Software and Systems V, ed. G. H. Jacoby & J. Barnes, 17

Böhringer, H., Briel, U. G., Schwarz, R. A., et al. 1994, Nature, 368, 828, doi: 10.1038/368828a0

Cappelluti, N., Li, Y., Ricarte, A., et al. 2017, ApJ, 837, 19, doi: 10.3847/1538-4357/aa5ea4

de Vaucouleurs, G. 1961, ApJS, 6, 213, doi: 10.1086/190064

Kaaret, P., Zajczyk, A., & D., L. 2019, in American Astronomical Society Meeting Abstracts, Vol. 53, American Astronomical Society Meeting Abstracts, 330.06

Liu, W., Chiao, M., Collier, M. R., et al. 2017, ApJ, 834, 33, doi: 10.3847/1538-4357/834/1/33

Planck Collaboration, Ade, P. A. R., Aghanim, N., et al. 2014, A&A, 571, A1, doi: 10.1051/0004-6361/201321529

Smith, R. K., Brickhouse, N. S., Liedahl, D. A., & Raymond, J. C. 2001, ApJL, 556, L91, doi: 10.1086/322992

Su, Y., Kraft, R. P., Nulsen, P. E. J., et al. 2019, AJ, 158, 6, doi: 10.3847/1538-3881/ab1d51

Tonry, J. L., Dressler, A., Blakeslee, J. P., et al. 2001, ApJ, 546, 681, doi: 10.1086/318301

Urban, O., Werner, N., Simionescu, A., Allen, S. W., & Böhringer, H. 2011, MNRAS, 414, 2101, doi: 10.1111/j.1365-2966.2011.18526.x

Wilms, J., Allen, A., & McCray, R. 2000, ApJ, 542, 914, doi: 10.1086/317016

Zhu, H., Tian, W., Li, A., & Zhang, M. 2017, MNRAS, 471, 3494, doi: 10.1093/mnras/stx1580